KARYA ILHAM PUBLISHING
CONNECTING MINDS, BRIDGING IDEAS, INSPIRING READERS

Advances in Fluid, Heat and Materials Engineering

Journal homepage:
https://karyailham.com.my/index.php/afhme/index
ISSN: 3083-8134

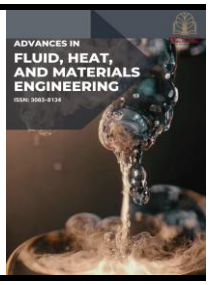

Analysis of External Flow Dynamics for Flow Over a Smooth Cube

Mohd Syahir Abd Razak[1,*]

[1] Department of Mechanical Engineering, Faculty of Mechanical Engineering and Manufacturing, Universiti Tun Hussein Onn Malaysia, 86400 Batu Pahat, Johor, Malaysia

ARTICLE INFO

Article history:
Received 4 June 2025
Received in revised form 1 July 2025
Accepted 16 July 2025
Available online 29 September 2025

Keywords:
Computational fluid dynamics; flow separation; drag coefficient; bluff body; smooth cube; external flow; Reynolds-averaged Navier–Stokes; k–omega turbulence model

ABSTRACT

The analysis of external flow around bluff bodies such as cubes is fundamental in fluid dynamics and engineering design. When air flows over sharp edges and corners, it tends to separate from the surface, which greatly affects how much drag the object experiences, the shape of the airflow behind it, and how pressure is spread around it. This study investigates how airflow separates and creates wakes around the edges of smooth cubes of different sizes when exposed to various velocities. Not fully understanding this flow can result in less efficient designs, greater drag, and higher energy use in engineering applications. The aim of this project is to investigate how air flows around smooth cubes, especially looking at how the flow separates, and to measure the drag force and drag coefficient under different conditions. Three different cube sizes 0.006 m, 0.008 m, and 0.010 m were studied, each tested at three airflow speeds: 10 m/s, 20 m/s, and 30 m/s. Using CFD in ANSYS Fluent, the steady, incompressible Navier Stokes equations were solved with the standard k ω turbulence model. The study looked at how velocity and pressure changed, examined airflow patterns, and measured drag performance for all the setups. Results showed that both the drag force and drag coefficient grew as the cube size and airflow speed increased. The largest cube (0.01 m) experienced the highest drag force, while the smallest cube (0.006 m) faced the least resistance. Flow separation consistently happened at the back corners and side edges, with longer and stronger wakes forming when the airflow was faster and the cubes were larger. The CFD analysis met the study's goals by measuring drag and clearly showing how the cube's shape and airflow speed work together to affect the flow patterns around it.

1. Introduction

Flow around blunt shapes like cubes have been widely researched because it plays a crucial role in many engineering fields, such as building aerodynamics, ventilation systems, and structural design [1,2]. These shapes interrupt the flow of air, causing the boundary layer to separate, creating vortices, and increasing aerodynamic drag [3]. When the flow separates behind a cube, it creates a low-pressure area called a wake, which affects the forces on the cube and leads to unsteady, changing flow patterns [4]. How fluid moves around a smooth cube is important for many real-world uses, such

* *Corresponding author.*
E-mail address: cd210011@student.uthm.edu.my

https://doi.org/10.37934/afhme.6.1.113a

as cooling electronics and studying structures in engineering. The cube's shape influences the flow, which affects the patterns of movement, heat transfer, and turbulence in the fluid.

Earlier research has found that the flow mainly separates at the back edges and corners of a cube because of its sharp shape and the way pressure changes around [5]. However, most previous studies have focused on just one size of geometry, used fixed Reynolds numbers, or concentrated mainly on experiments and unsteady simulation methods like LES [6,7]. Aslan *et al.,* [8] used large eddy simulation (LES) to show how adding vortex generators can boost the cooling of surface-mounted cubes by altering the airflow around them. They simple design tweaks, like adding chamfers to the tops of electronic components, can noticeably change the way air flows around them, which then impacts how effectively those parts are cooled [9].

The aim of this study is to explore how fluid flows around a smooth cube using computational fluid dynamics (CFD), focusing especially on how the flow separates at the cube's edges and corners [10]. The study will look at factors like drag force, drag coefficient (Cd), pressure drop, and how the wake forms at different speeds and shapes under turbulent flow conditions [11]. This fits well with your interest in fluid dynamics and improving cooling performance. Three cubes of different sizes 0.006 m, 0.008 m, and 0.010 m were modelled and positioned inside a uniform rectangular space for analysis. This matches your interest in fluid dynamics and CFD around cubes. CFD simulations were carried out using steady-state incompressible Navier Stokes equations, applying the standard k–ω turbulence model within ANSYS Fluent [12]. Each cube size was tested at three different inlet speeds 10, 20, and 30 m/s. A carefully structured grid with finer mesh around the cube was used, and the simulations were considered complete once the residuals dropped below 10^{-4}.

Key reference values like velocity, frontal area, and fluid density were defined to ensure precise calculation of the drag coefficient (Cd) and other flow-related variables. The results reveal that as the cube gets bigger and the flow speed rises, both the drag force and drag coefficient (Cd) increase. Streamline visuals clearly show separation zones starting from the cube's back edges and top corners [13-15]. Simulations like those done by previous researchers highlighted how crucial it is to carefully set up simulations and consider surface conditions to accurately predict how flow separates around cubes mounted on walls [16-18]. Simulation results met the study's goals by clearly showing how flow separates around different cube sizes and speeds. The CFD method used successfully captured important aerodynamic features seen in previous research, confirming that the computational setup is reliable for studying bluff bodies [19,20].

2. Methodology

2.1 Geometry Construction

This study investigates how air flows around three different cube sizes placed in a steady airflow, as shown in Figure 1. The cubes vary in size, a small one measuring 0.006 meters on each side (D1), a medium one at 0.008 meters per side (D2), and a larger cube with sides of 0.010 meters (D3). These cube sizes were chosen to study how the front-facing area and overall size influence the way air separates and creates drag around the cubes at different flow speeds. Each cube is positioned right in the middle of a rectangular space where the airflow is set to fixed dimensions, 0.08 meters long (z-direction), 0.03 meters wide (x-direction), and 0.03 meters height (y-direction). The size of this space was carefully picked to give enough room for the airflow to develop before reaching the cube, allow the wake behind the cube to form properly, and avoid any interference from the walls of the domain (Figure 2).

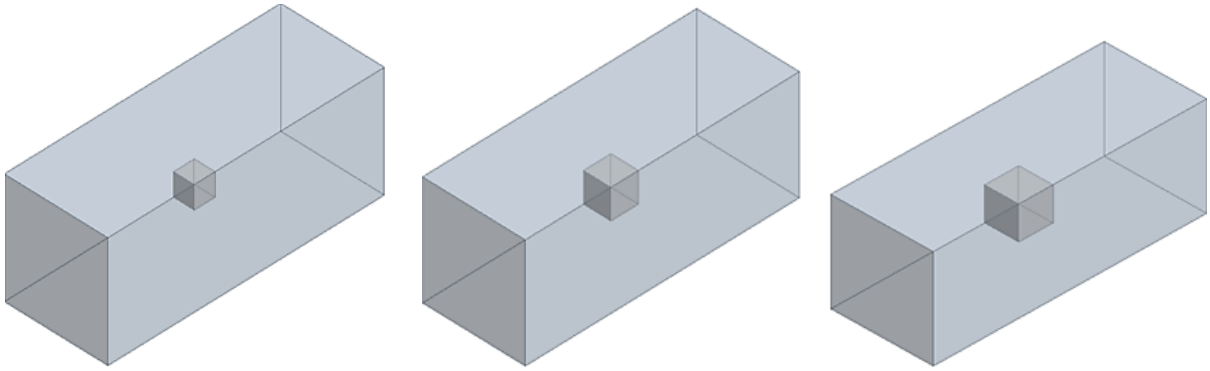

(a) (b) (c)

Fig. 1. The geometry of cube (a) 0.006 m each side (b) 0.008 m each side (c) 0.010 m each side

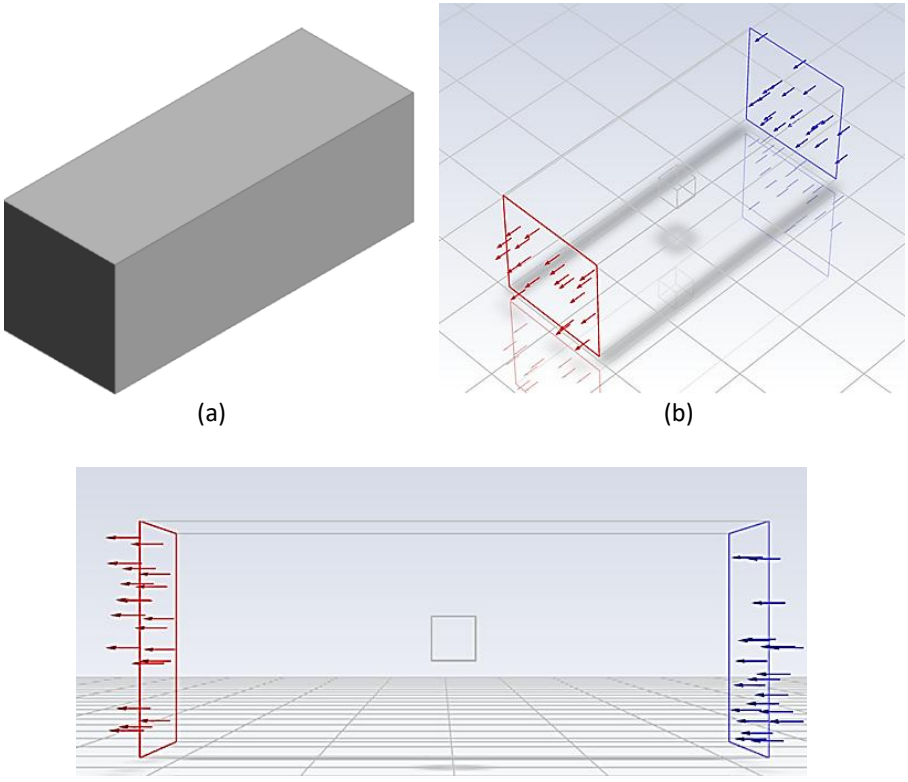

(a) (b)

(c)

Fig. 2. (a) Geometry of airflow (b) Isometric view of airflow domain showing inlet and outlet flow (c) Side view of airflow domain with central cube

2.2 Meshing

Meshing was performed using unstructured tetrahedral elements in ANSYS Meshing for all three cube geometries which are D1, D2 and D3. Local refinement was applied near the cube surface to capture important flow features such as boundary layer separation and wake formation. The element size was varied slightly to evaluate the effect of mesh resolution across three refinement levels. Each cube size (D1 = 0.006 m, D2 = 0.008 m, and D3 = 0.010 m) was meshed using the same consistent method. The total number of mesh nodes for each cube, depending on the different element sizes used, is detailed in Table 1. The mesh quality was evaluated by checking skewness and orthogonal quality, and all meshes met the standards recommended by ANSYS Fluent. The mesh was created without adaptive sizing, using a consistent growth rate of 1.2 throughout the domain. An example of the generated mesh for the D3 cube (0.010 m) is shown in Figure 3.

Table 1
Mesh configuration for each cube geometry

Diameter (m)	Element size (m)	Number of nodes
0.006	0.0029	4,069
	0.0027	4,759
	0.0025	5,597
0.008	0.0029	4,106
	0.0027	4,820
	0.0025	5,640
0.010	0.0029	4,088
	0.0027	4,791
	0.0025	5,704

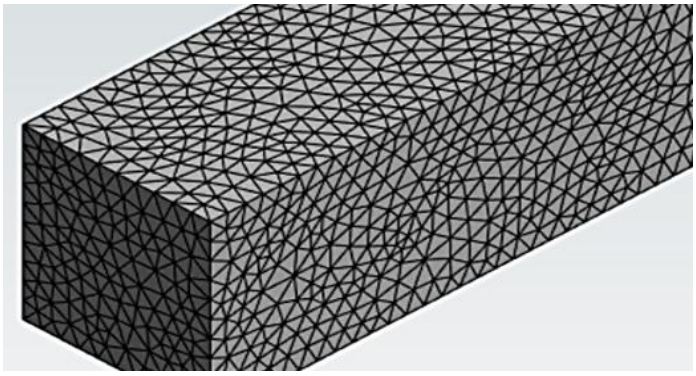

Fig. 3. Tetrahedral mesh applied to the D3 cube geometry using ANSYS Meshing (element size = 0.0029 m)

2.3 Governing Equation

The airflow around the smooth cubes is described by basic fluid dynamics equations, including the continuity equation to ensure mass conservation and the Navier Stokes equations for momentum. Since the flow is considered incompressible, steady, and turbulent, these equations were solved using the Reynolds-Averaged Navier Stokes (RANS) method along with a turbulence model to accurately capture the effects of turbulence. For incompressible flow, the conservation of mass is expressed as shown in Eq. (1). While, the momentum conservation for incompressible and turbulent airflow is expressed in Eq. (2).

$$\nabla \cdot \vec{v} = 0 \tag{1}$$

$$\rho\left(\frac{\delta \vec{v}}{\delta t} + \vec{v} \cdot \nabla \vec{v}\right) = -\nabla \rho + \mu \nabla^2 \vec{v} + \vec{F} \tag{2}$$

2.4 Boundary Conditions

This simulation looks at how air flows around a stationary cube inside a closed rectangular space. The airflow is considered incompressible, steady, and fully turbulent. To accurately capture the behaviour near the cube's surface and the way the flow separates around it, the standard k–ω turbulence model was used throughout the simulations. The same boundary conditions were applied consistently for all three cube sizes and across the three different inlet velocities. A summary of these boundary conditions can be found in Table 2. These boundary conditions were applied the same way across all nine simulation scenarios, covering the three cube sizes and three different inlet speeds.

The external domain was designed to be large enough to reduce any blockage effects and to let the wake form naturally behind each cube.

Table 2
Boundary conditions and solver parameters

Description	Setting/type
Flow type	External, Steady-state, incompressible
Turbulence model	Standard k-ω
Inlet boundary	Velocity inlet: 10,20, and 30m/s; turbulence intensity = 5%
Outlet boundary	Pressure outlet: 0 Pa (gauge pressure)
Cube surface	Wall (no-slip, stationary)
Top and bottom walls	Symmetry
Side walls (left/right)	Symmetry
Initialisation	From inlet
Iteration limit	Up to 1000 iterations per case

2.5 Analysis

Once each simulation reached convergence, the results were processed using ANSYS Fluent to extract and analyze key flow characteristics. The focus was on examining how the flow separates around the cubes, as well as calculating the drag force and drag coefficient (Cd) for each cube size and inlet velocity. This post-processing step helped to understand the flow behaviour and aerodynamic performance in detail. The total drag force on the cube was calculated using the Forces Report feature in ANSYS Fluent, while the drag coefficient was automatically determined through the Force Coefficient Report based on reference values like the cube's frontal area, fluid density, and inlet velocity. To visualize the flow behaviour, contour plots showing velocity magnitude and static pressure were created, highlighting how the flow speeds up and how pressure varies over the cube's surface and in the wake behind it. Additionally, streamline plots were used to observe flow separation, vortex formation, and the length of the wake trailing the cube. This combination of quantitative data and visualizations helped provide a clear understanding of the airflow patterns and aerodynamic forces involved.

Pressure probes were also placed upstream and downstream of the cube to measure the pressure drop and check that these readings matched the drag data. Throughout the simulations, residuals for continuity, momentum, and turbulence were closely monitored, and the solution was considered converged once all residuals dropped below 1×10^{-4} and the drag coefficient stabilized. These visual and numerical results formed the basis for further analysis and comparison with existing published data in the following section of the report.

3.0 Results and Discussion

3.1 Grid Independence Test (GIT)

A grid independence test was performed to make sure the simulation results weren't significantly affected by the size of the mesh. This step is important in CFD studies to balance accuracy with computational efficiency. By comparing the drag coefficient (Cd) from three different mesh densities for the largest cube, the study confirmed that the selected mesh was detailed enough, as refining it further caused only minor changes in the results. This ensured accurate outcomes without wasting extra computing time.

3.1.1 Velocity chart

Figure 4 shows the velocity distribution results from the grid independence test for different cube sizes (0.006 m, 0.008 m, and 0.010 m). The comparison reveals that the velocity values stay consistent regardless of the mesh density, which means the chosen mesh is detailed enough to ensure accurate and reliable flow simulations.

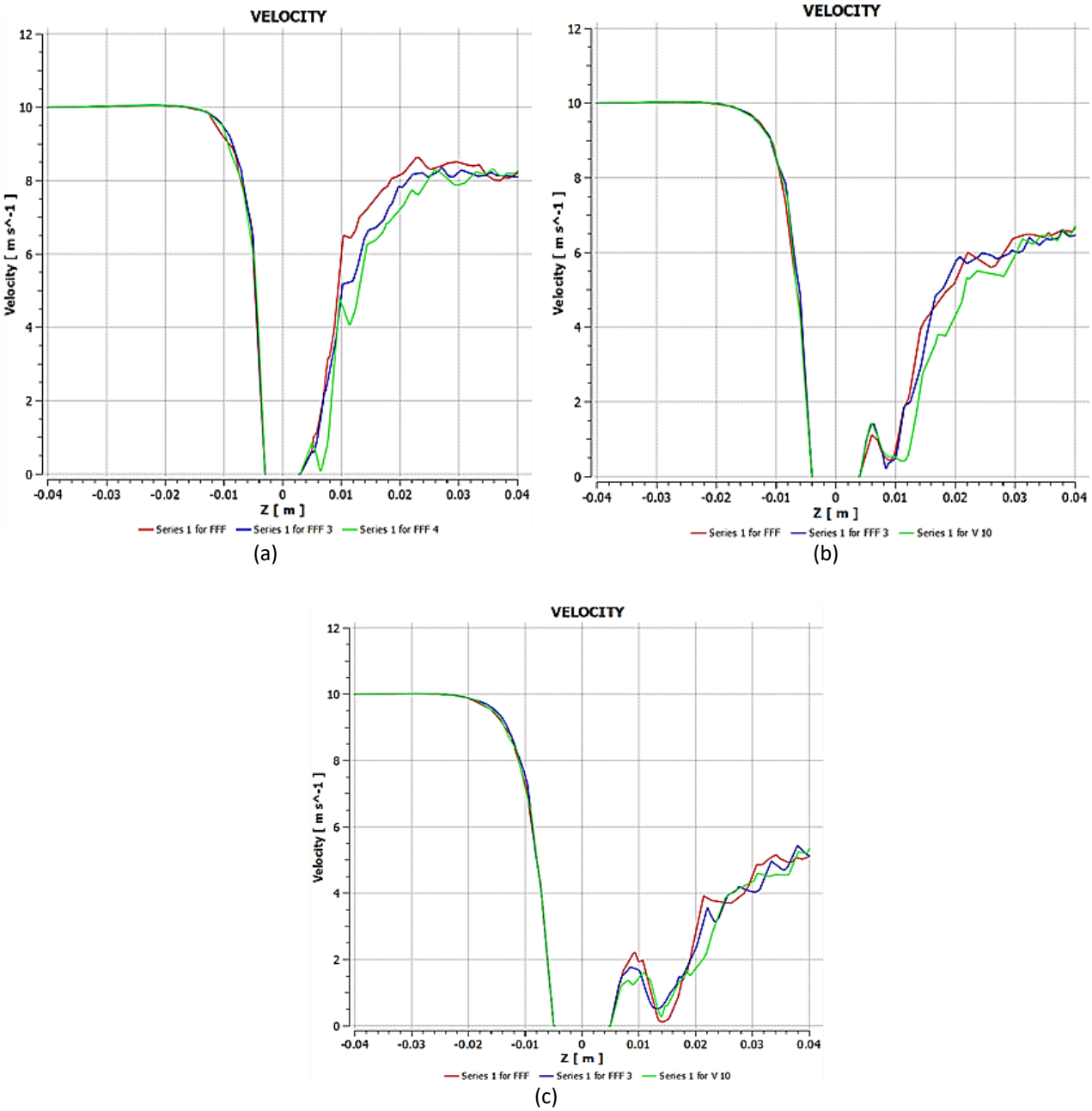

Fig. 4. The GIT chart of velocity for smooth cube (a) 0.006 m (b) 0.008 m (c) 0.010 m

3.1.2 Pressure chart

Figure 5 illustrates how pressure changes with different mesh resolutions during the grid independence test. The pressure values show very little difference across the various element sizes, confirming that the pressure results are reliable and not affected by the mesh size.

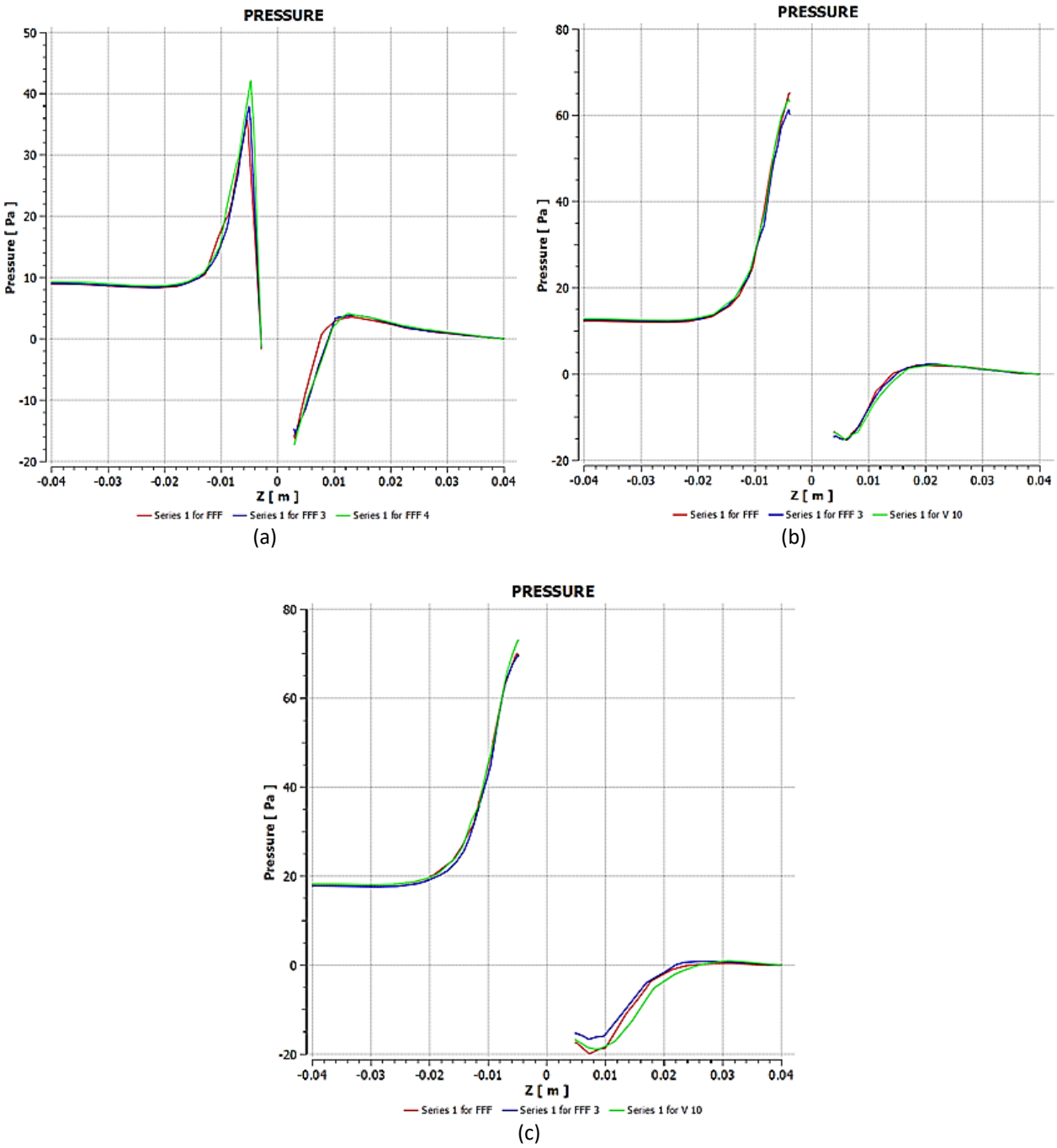

Fig. 5. The GIT chart of pressure for smooth cube (a) 0.006 m (b) 0.008 m (c) 0.010 m

3.1.3 Turbulence kinetic energy

Figure 6 displays the turbulent kinetic energy (TKE) results for each cube size at different mesh densities. The consistent TKE values across these meshes confirm that the chosen mesh resolution effectively captures the turbulence in the flow.

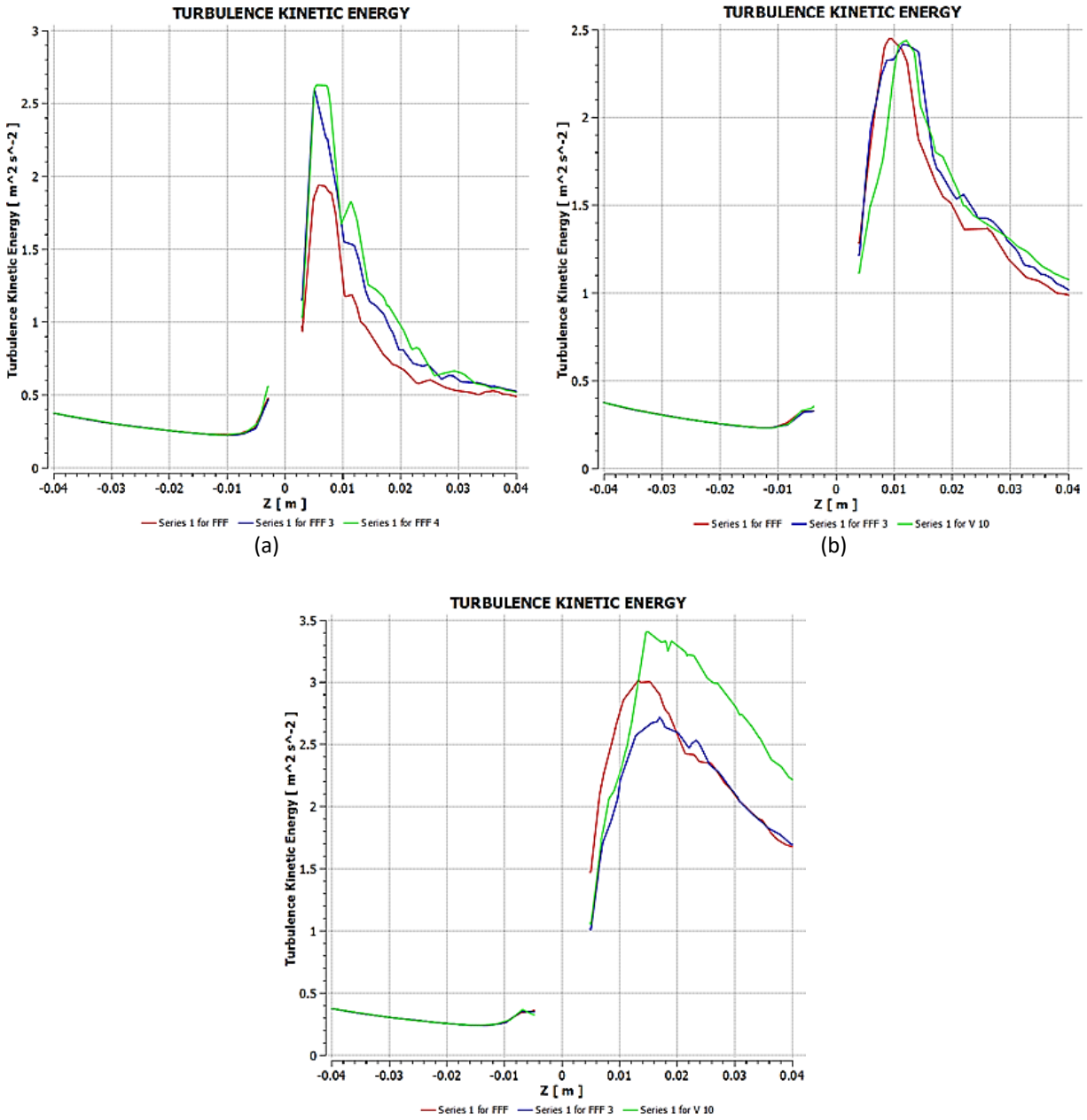

Fig. 6. The GIT chart of turbulence kinetic energy for smooth cube (a) 0.006 m (b) 0.008 m (c) 0.010 m

3.2 Velocity Streamlines

Figures 7 to 9 illustrate the velocity streamlines around the cube shapes for sizes D1 (0.006 m), D2 (0.008 m), and D3 (0.010 m) at inlet speeds of 10 m/s, 20 m/s, and 30 m/s. In every case, the flow starts to separate at the back edges of the cubes, becoming more noticeable as both the velocity and cube size increase. For the smallest cube, the wake behind it is short and narrow, while the largest cube creates a longer, more turbulent wake. The streamline patterns clearly show stronger vortex shedding and larger recirculation zones as the Reynolds number goes up.

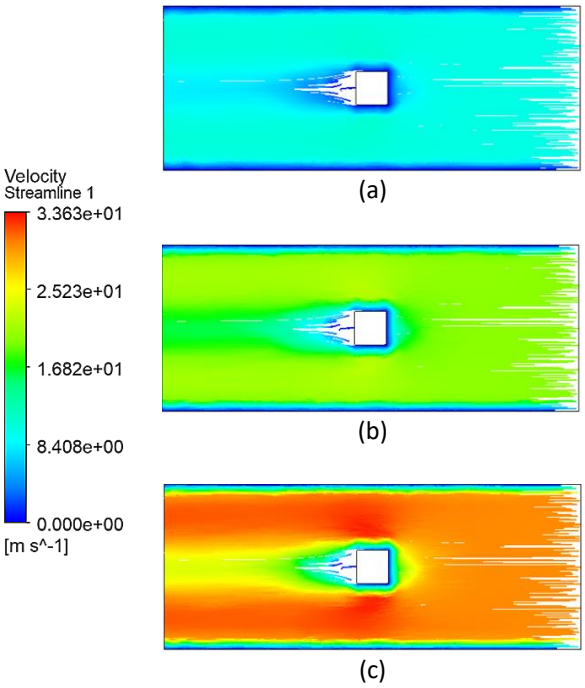

Fig. 7. The visual of velocity streamlines for smooth cube diameter 0.006 m (a) Velocity 10 m/s (b) Velocity 10 m/s (c) Velocity 30m/s

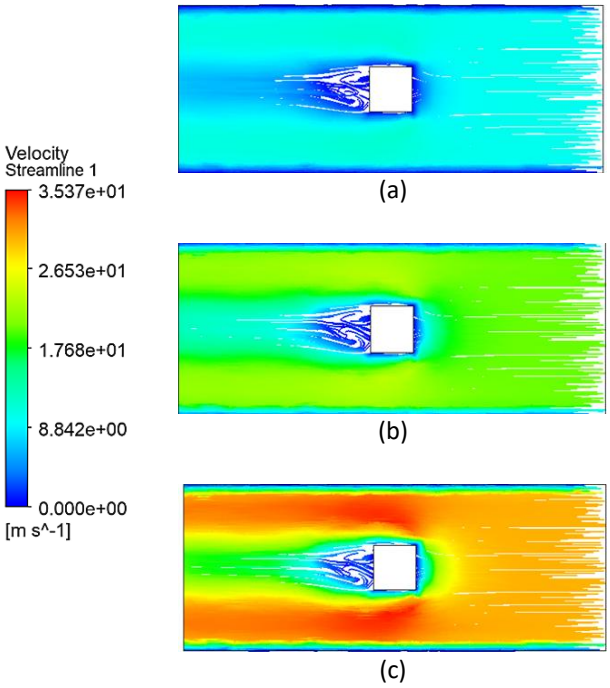

Fig. 8. The visual of velocity streamlines for smooth cube diameter 0.008 m (a) Velocity 10 m/s (b) Velocity 10 m/s (c) Velocity 30 m/s

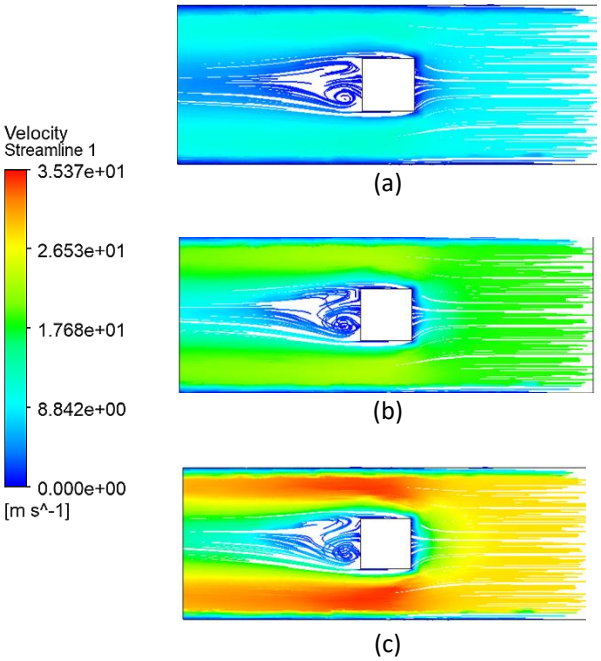

Fig. 9. The visual of velocity streamlines for smooth cube diameter (a) Velocity 10m/s (b) *V*elocity 10m/s (c) Velocity 30m/s

3.3 Contour Pressure

Figures 10 to 12 show the static pressure contours around each cube shape. In every case, there's a high-pressure area at the front of the cube where the airflow slows down, followed by a low-pressure zone at the back caused by flow separation. As the cube size and velocity increase, the

pressure changes become more pronounced, leading to a bigger pressure drop across the cube. This pressure pattern directly affects the drag force on the cube and highlights how the shape of a bluff body impacts the resistance it experiences from the flow.

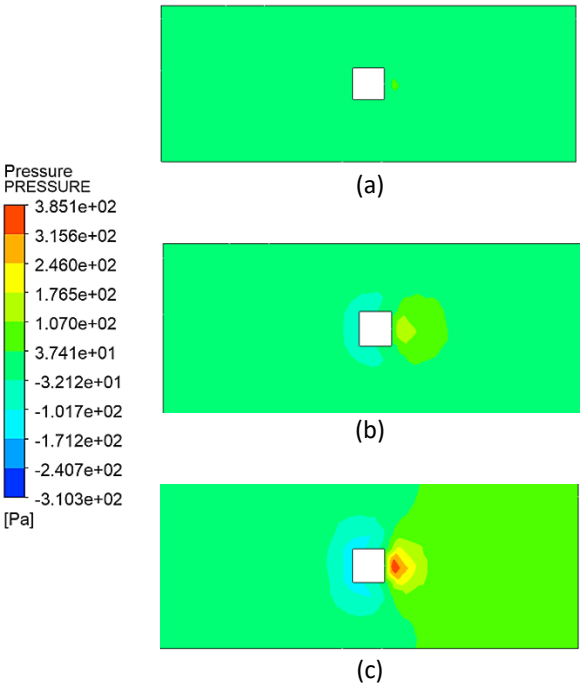

Fig. 10. The visual of contour pressure for smooth cube diameter 0.006 m (a) Velocity 10 m/s (b) Velocity 10 m/s (c) Velocity 30 m/s

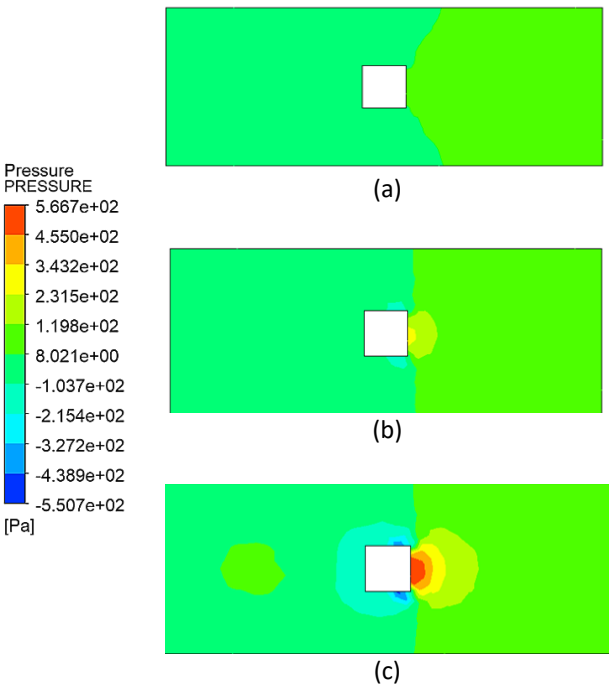

Fig. 11. The visual of contour pressure for smooth cube diameter 0.008m (a) Velocity 10 m/s (b) Velocity 10 m/s (c) Velocity 30 m/s

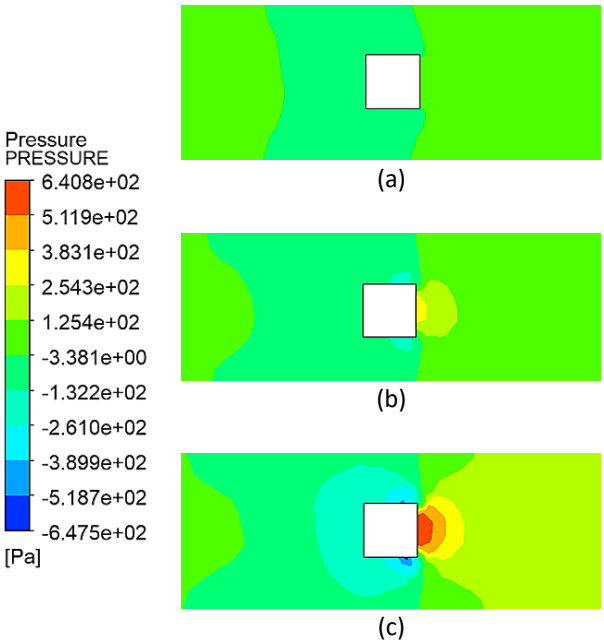

Fig. 12. The visual of contour pressure for smooth cube diameter 0.010 m (a) Velocity 10 m/s (b) Velocity 10 m/s (c) Velocity 30 m/s

3.4 Contour Turbulence Kinetic Energy

Figures 13 to 15 display the turbulent kinetic energy (TKE) contours for the three different cube sizes. The TKE distribution shows low turbulence levels in front of the cubes, while turbulence intensifies in the wake behind them, especially at higher speeds. As the cube size grows, the wake becomes larger and more energetic, with turbulence spreading further downstream. This clearly shows how both the size of the obstacle and the flow velocity work together to shape and strengthen the turbulent patterns in the flow.

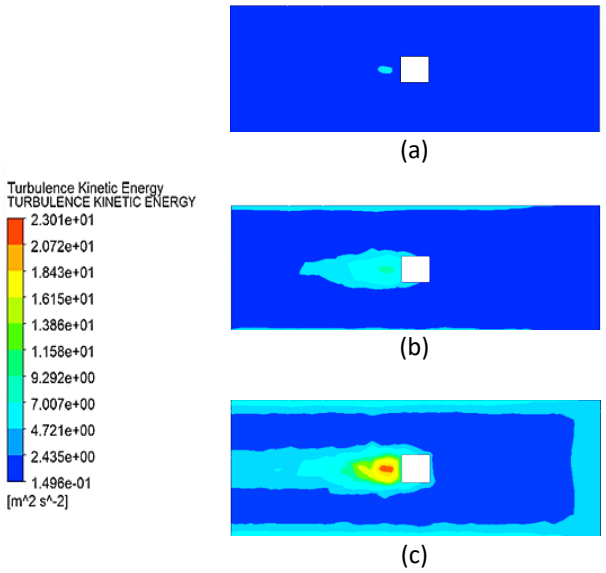

Fig. 13. The visual of contour turbulence kinetic for smooth cube diameter 0.006 m (a) Velocity 10 m/s (b) Velocity 10 m/s (c) Velocity 30 m/s

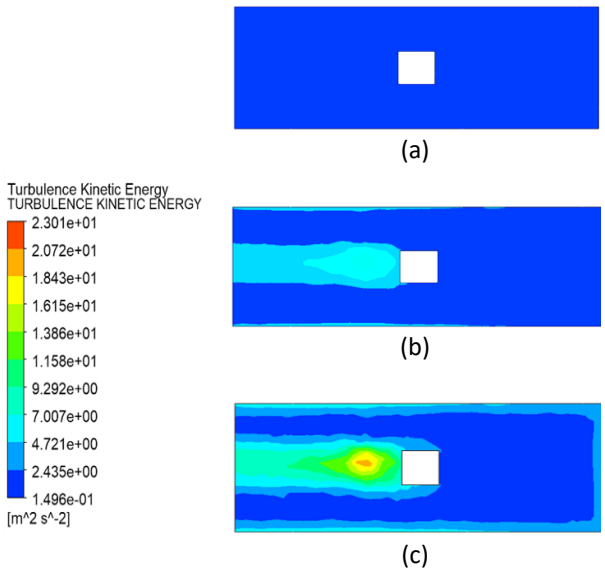

Fig. 14. The visual of contour turbulence kinetic for smooth cube diameter 0.008 m (a) Velocity 10 m/s (b) Velocity 10 m/s (c) Velocity 30 m/s

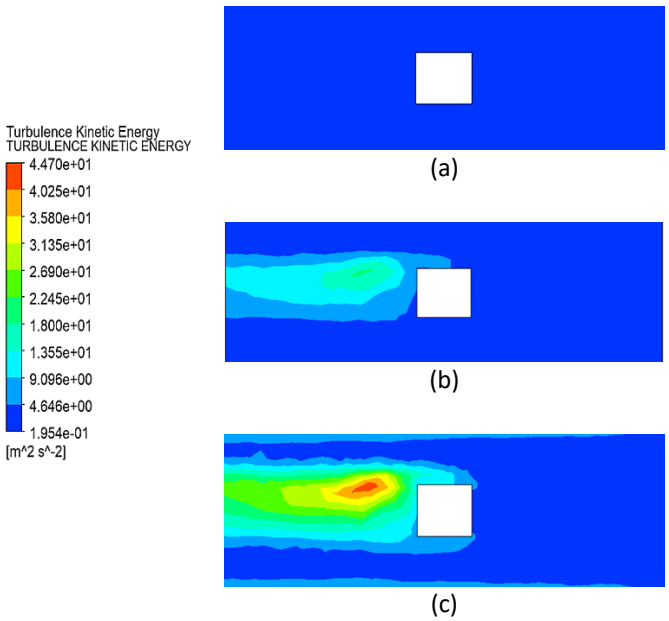

Fig. 15. The visual of contour turbulence kinetic for smooth cube diameter 0.010 m (a) Velocity 10 m/s (b) Velocity 10 m/s (c) Velocity 30 m/s

4. Conclusions

This study explored how air flows around smooth cubes of different sizes (0.006 m, 0.008 m, and 0.010 m) at various inlet speeds (10 m/s, 20 m/s, and 30 m/s) using CFD simulations in ANSYS Fluent. By solving the steady-state incompressible Navier–Stokes equations with the standard k–ω turbulence model, we were able to examine key flow features like separation, wake development, and how these affect the drag force and drag coefficient on the cubes.

The results revealed that both the drag force and drag coefficient grew as the cube size and airflow speed increased. Flow separation consistently happened at the back edges and top corners of the cubes, with bigger cubes and faster air creating longer more turbulent wakes. The velocity streamlines and pressure contours clearly showed the formation of recirculation zones and sharp pressure changes across the cube surfaces. Additionally, the turbulent kinetic energy plots highlighted stronger turbulence in the wake area as the cube size and Reynolds number went up.

The grid independence test confirmed that the selected mesh resolution was detailed enough to accurately capture important flow characteristics without losing precision. Overall, the simulation results successfully met the research goals by measuring aerodynamic behavior and clearly showing flow separation patterns. This study demonstrates that CFD is a powerful and reliable method for studying bluff body aerodynamics, emphasizing how both the shape of the object and the flow conditions play a crucial role in its aerodynamic performance.

References

[1] Langston, Craig, Francis KW Wong, Eddie CM Hui, and Li-Yin Shen. "Strategic assessment of building adaptive reuse opportunities in Hong Kong." *Building and Environment* 43, no. 10 (2008): 1709-1718. https://doi.org/10.1016/j.buildenv.2007.10.017

[2] Kim, Sangil, Md Mahbub Alam, Hiroshi Sakamoto, and Yu Zhou. "Flow-induced vibration of two circular cylinders in tandem arrangement. Part 2: Suppression of vibrations." *Journal of Wind Engineering and Industrial Aerodynamics* 97, no. 5-6 (2009): 312-319. https://doi.org/10.1016/j.jweia.2009.07.003

[3] Launder, B. E. "Turbulent Jets. By N. Rajaratnam. Elsevier, 1976. 304 pp.£ 23.45." *Journal of Fluid Mechanics* 82, no. 3 (1977): 607-608. https://doi.org/10.1017/S0022112077220866

[4] Li, Jiawei, Xiaolei Han, Hiroka Rinoshika, Wenming Li, and Akira Rinoshika. "Flow control of wake around a wall-mounted cube using a horizontal hole of different diameters." *Physics of Fluids* 34, no. 3 (2022). https://doi.org/10.1063/5.0082878

[5] Premnath, Kannan N., Martin J. Pattison, and Sanjoy Banerjee. "Computation of transitional flow past a circular cylinder using multiblock lattice Boltzmann method with a dynamic subgrid scale model." *Fluid Dynamics Research* 45, no. 5 (2013): 055510. https://doi.org/10.1088/0169-5983/45/5/055510

[6] Constantinescu, George S., Hugo Pasinato, You-Qin Wang, James R. Forsythe, and Kyle D. Squires. "Numerical investigation of flow past a prolate spheroid." *Journal of Fluids Engineering* 124, no. 4 (2002): 904-910. https://doi.org/10.1115/1.1517571

[7] Li, Aiqin, and Earl H. Dowell. "Modal reduction of mathematical models of biological molecules." *Journal of Computational Physics* 211, no. 1 (2006): 262-288. https://doi.org/10.1016/j.jcp.2005.05.021

[8] Aslan, Necdet, Esin Onbaşıog˘lu, Şölen Balcı, and Adem Erdoğan. "Parallelizaton of visual magneto-hydrodynamics code based on fluctuation distribution scheme on triangular grids." *Computers & Fluids* 36, no. 5 (2007): 961-973. https://doi.org/10.1016/j.compfluid.2006.05.004

[9] Hatef, Ali, Simon Fortin-Deschênes, Etienne Boulais, Frédéric Lesage, and Michel Meunier. "Photothermal response of hollow gold nanoshell to laser irradiation: Continuous wave, short and ultrashort pulse." *International Journal of Heat and Mass Transfer* 89 (2015): 866-871. https://doi.org/10.1016/j.ijheatmasstransfer.2015.05.071

[10] Kumar, Ashwini, and Ilhan Dilber. "Fluid flow and its modeling using computational fluid dynamics." In *Handbook of Food and Bioprocess Modeling Techniques*, pp. 41-87. CRC Press, 2006. https://doi.org/10.1201/9781420015072-4

[11] Warholic, Michael D., Gavin M. Schmidt, and Thomas J. Hanratty. "The influence of a drag-reducing surfactant on a turbulent velocity field." *Journal of Fluid Mechanics* 388 (1999): 1-20. https://doi.org/10.1017/S0022112099004498

[12] Wilcox, David C. "Formulation of the kw turbulence model revisited." *AIAA journal* 46, no. 11 (2008): 2823-2838.
[13] Li, Aiqin, and Earl H. Dowell. "Modal reduction of mathematical models of biological molecules." *Journal of Computational Physics* 211, no. 1 (2006): 262-288. https://doi.org/10.1016/j.jcp.2005.05.021
[14] Prasad, Anil, and Charles HK Williamson. "The instability of the shear layer separating from a bluff body." *Journal of Fluid Mechanics* 333 (1997): 375-402. https://doi.org/10.1017/S0022112096004326
[15] Menter, Florian R. "Two-equation eddy-viscosity turbulence models for engineering applications." *AIAA Journal* 32, no. 8 (1994): 1598-1605. https://doi.org/10.2514/3.12149
[16] Lowe, K. Todd, and Roger L. Simpson. "Measurements of velocity–acceleration statistics in turbulent boundary layers." *International Journal of Heat and Fluid Flow* 27, no. 4 (2006): 558-565. https://doi.org/10.1016/j.ijheatfluidflow.2006.02.003
[17] Chou, Yin, and Ruey-Jen Yang. "Two-dimensional dual-phase-lag thermal behavior in single-/multi-layer structures using CESE method." *International Journal of Heat and Mass Transfer* 52, no. 1-2 (2009): 239-249. https://doi.org/10.1016/j.ijheatmasstransfer.2008.06.025
[18] Avnaim, M. H., B. Mikhailovich, A. Azulay, and A. Levy. "Numerical and experimental study of the traveling magnetic field effect on the horizontal solidification in a rectangular cavity part 1: Liquid metal flow under the TMF impact." *International Journal of Heat and Fluid Flow* 69 (2018): 23-32. https://doi.org/10.1016/j.ijheatfluidflow.2017.11.003
[19] Cheeseman, I. C. "Fluid-dynamic drag: Practical information on aerodynamic drag and hydrodynamic resistance. SF Hoerner. Hoerner Fluid Dynamics, Brick Town, New Jersey. 1965. 455 pp. Illustrated. $24.20." *The Aeronautical Journal* 80, no. 788 (1976): 371-371. https://doi.org/10.1017/S0001924000034187
[20] Bearman, Peter W. "Vortex shedding from oscillating bluff bodies." *Annual Review of Fluid Mechanics* 16 (1984): 195-222. https://doi.org/10.1146/annurev.fl.16.010184.001211